Calibration And Validation Of An Airborne Hyperspectral Scanning Imager For Agricultural Missions

Mara Alain Maestro[1], Micherene Clauzette Lofamia, Ralph Aaron Aguinaldo, Andrew Rafael Bañas, and Maricor Soriano
National Institute of Physics, University of the Philippines Diliman, 1101 Quezon City, Philippines,
[1]Email: mmmaestro1@up.edu.ph

KEY WORDS: pushbroom, scanning, hyperspectral, calibration, validation

ABSTRACT: Hyperspectral remote sensing has been in wide use for agricultural monitoring. Its high spectral resolution enables better characterization of crops and other vegetation. Airborne scanning scientific cameras present an advantage of having a readily deployable instrument that can get zero cloud cover and high spatial resolution over the targets for applications such as monitoring or detecting changes right after calamities. With these merits, we designed and assembled a hyperspectral scanning camera called "Hypie" from commercial off-the-shelf (COTS) components. This paper reports the laboratory radiometric calibration done with the sensor in order to recover the spectral information and convert the digital numbers into radiance units. An outdoor experiment is done to capture vegetation spectra and sun irradiance. Three (3) sets of calibration constants are calculated and are validated against a commercial spectrometer. The maximum absolute error and root mean square error values computed range from 0.599 to 1.470 x 10^{-4} W/m^2-sr-nm and from 0.775 to 1.689 x 10^{-4} W/m^2-sr-nm respectively.

1. INTRODUCTION

Remote sensing has been a popular technological solution to enable observation of vast areas of lands within a short amount of time. The utilization and analysis that can be done on gathered spectral information is helpful in monitoring vegetation and managing agriculture. One of the challenges in utilizing remotely sensed optical data is its ability to preserve the spectrum. With a typical multispectral camera, wide bandwidths might not be enough to effectively observe the target's desired properties. In such a case, hyperspectral remote sensing provides an advantage (Maes, Steppe, 2019).

We developed an airborne pushbroom scanning hyperspectral imager called "Hypie" for agricultural missions. It is assembled from commercially available components and is easily deployable via drone. This paper aims to discuss the laboratory calibration and outdoor validation done to the assembly to ensure its data reliability and to effectively convert the raw DN values into physical units, in this case, radiance.

For the calibration, an integrating sphere illuminated with a calibration incandescent lamp was used in the laboratory. Before any comparison was made between the assembled image and a commercial spectrometer, an image processing workflow was implemented to minimize the effects of the camera's intrinsic characteristics of dark noise, non-uniformity, and transmittance limitation. Three sets of calibration coefficients were calculated from different calibration configurations. All these coefficients were tested for validation wherein a commercial reference spectrometer (Jaz Ocean Optics) is used simultaneously with Hypie. Five (5) vegetation targets and sun radiance were measured outdoors.

2. OPTICAL ASSEMBLY

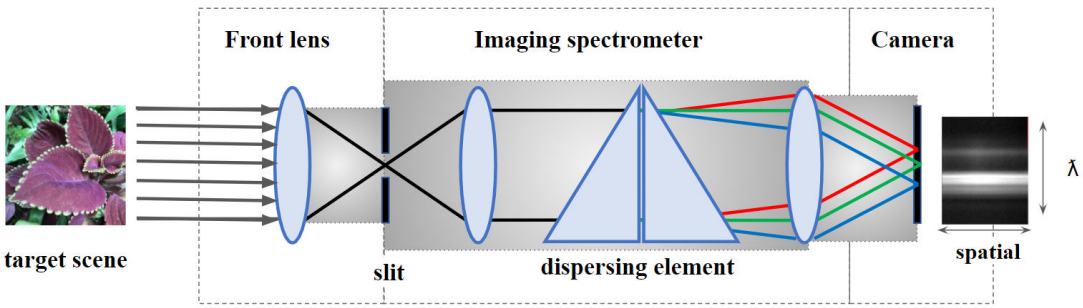

Figure 1. Hypie's optical assembly.

Hypie's is built from available commercial components. Its operating principle is visualized in Figure 1. A stock lens collects the radiant energy from the target scene and the entrance slit ensures that only a single line from the

object is imaged by the sensor. This line image is dispersed by a prism-grating-prism imaging spectrometer (SPECIM Imspector V10) into its wavelength components. A monochromatic CMOS USB camera (FLIR Ptgrey) captures this as a 2D image with spectral and spatial axes. FLIR's available software development kit is being utilized to operate the whole assembly.

Based on the CMOS's pixel count, Hypie has a total of 1280 spectral bands ranging from 271 to 1151 nm. It has been designed to have a 0.667 nm spectral interval. With a 50 μm slit, the sensor's effective spectral resolution is 6.95 nm. (Maestro, et.al., 2021).

3. DATA ACQUISITION

Two activities were launched to calibrate and validate Hypie's optical assembly. Controlled laboratory equipment is first used for calibration. An outdoor validation was done to capture vegetation and sun spectral data.

3.1 Laboratory Experiment

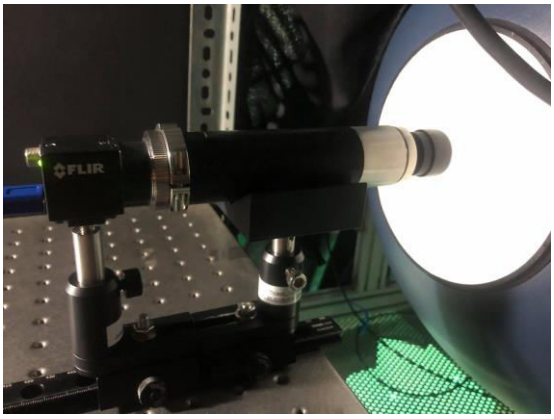

Figure 2. Hypie assembly set-up when acquiring integrating sphere captures. Room light is turned-off during the actual experiment.

An integrating sphere illuminated by a calibration incandescent lamp was utilized in doing the calibration of the corrected DN to physical units (radiance values) (see Figure 2). The calibration lamp was set to 7 current values effectively changing the spectral radiance and total power it emits (see Figure 3). For each current value, the Hypie's optical assembly was made to capture at 3 exposure time values (5, 6, and 7 ms) and 3 gain factor values (0, 0.5, and 1 dB). Multiple bright captures were made and averaged per each set of parameters. Dark captures were taken and mean bright images were computed accordingly.

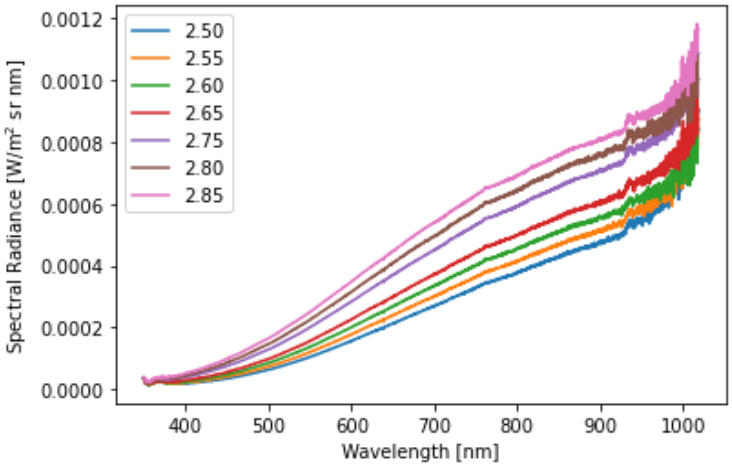

Figure 3. Spectral radiance of the set currents (in amperes) of the calibration lamp used for Hypie's calibration.

3.2 Validation Using Vegetation and Sun Spectrum

An agricultural field campaign was originally planned to validate the calibration. However, activity and local travel restrictions due to the COVID-19 pandemic hindered its progress. Instead, an outdoor validation was done wherein

five (5) vegetation radiance and sun irradiance measurements were acquired using a calibrated commercial spectrometer (Jaz Ocean Optics).

Figure 4. Plants' leaves A to E used as validation targets.

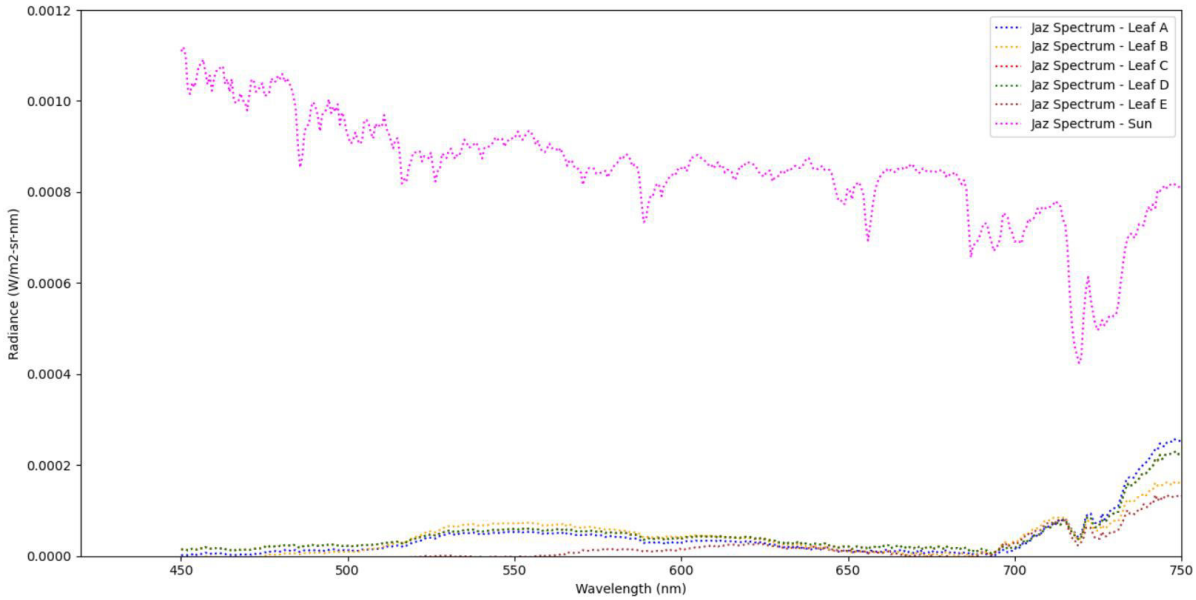

Figure 5. Gathered validation data set

Hypie and Jaz spectrometers were used to capture leaf targets simultaneously. A cosine corrector was utilized to capture the sun irradiance. The spectral data gathered are shown in Figure 5.

4. DATA PROCESSING

Prior to the actual computation of calibration constants, Hypie images are first radiometrically corrected. The corrected DN values were compared to the calibration lamp's radiance values and validated against the acquired vegetation and sun spectra.

4.1 Radiometric Correction

Hypie has been characterized by its dark noise, non-uniformity, and transmittance limitation - all are expected intrinsic properties of an optical imager. These may interfere in the consistency of the raw DN data across both the spatial and wavelength axes. In this section, we will discuss the processing workflow (Figure 6) developed and applied to each Hypie image to minimize such inconsistencies.

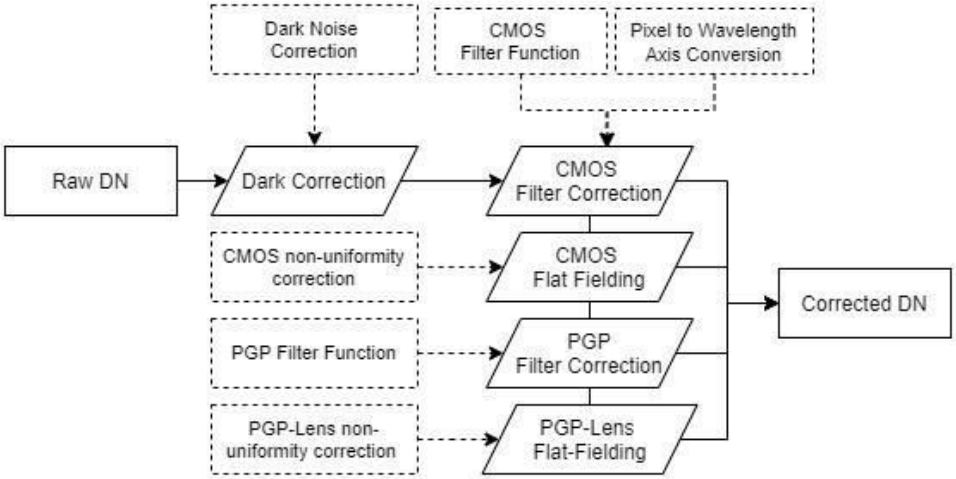

Figure 6. Radiometric correction workflow to correct the camera assembly's dark noise, non-uniformity and transmittance filter.

The correction applied to the raw images are summarized in the equation:

$$\square = \frac{\square - \square}{\Lambda_{\square\square\square\square} * \Lambda_{\square\square\square\square\square\square} * \square_1 * \square_2 * \square * \square} \quad (1)$$

where C is the corrected image DN, R is the raw image, $\Lambda_{\square\square\square\square}$ is the CMOS camera transmittance function, $\Lambda_{\square\square\square\square\square\square}$ is the imaging spectrometer transmittance function, $\square_1$ is the CMOS non-uniformity image, $\square_2$ is the imaging spectrometer and lens non-uniformity image, τ is the exposure time in ms and $\square$ is the gain factor. Small letters indicate scalar values while capital letters are arrays.

Dark Correction and Flat-Fielding: It is imperative to do dark noise correction to the images. The dark captures acquired per set of parameters were each subtracted from the flat image captures. Then, the non-uniformities were accounted for.

There are three components causing non-uniformity to Hypie's images - the CMOS sensor (FLIR Ptgrey), the imaging spectrometer (ImSpector), and the lens (Edmund Optics). The non-uniformity is removed using two derived image corrections. G_1 accounts for the CMOS non-uniformity while G_2 accounts for the collective non-uniformity of the imaging spectrometer and the lens (Lofamia, et. al., 2021).

Filter Correction: The assembly has two main filtering components - the CMOS sensor and the imaging spectrometer. The transmittance functions of each were taken into account and are applied as part of the radiometric correction. Since these data are wavelength sensitive, pixel axis to wavelength axis conversion (Maestro, et.al., 2021) must be done first. The transmittance filter corrections are incorporated in the equation as $\Lambda_{\square\square\square\square}$ and $\Lambda_{\square\square\square\square\square\square}$ respectively.

Each correction stage applied to Hypie's raw DN values is visualized in Figure 7.

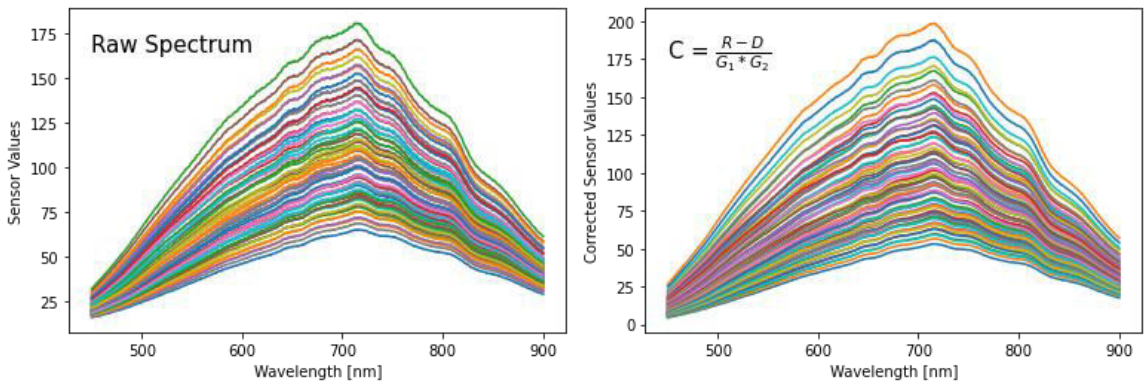

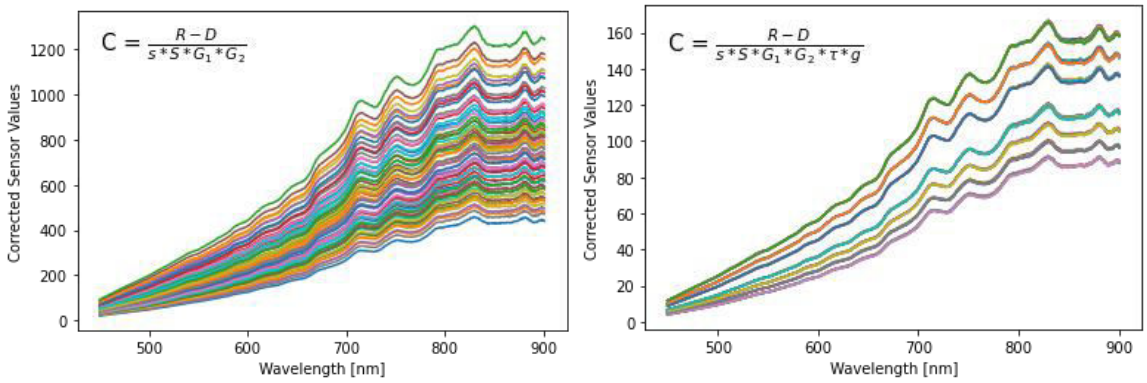

Figure 7. C($C = \frac{R-D}{\Lambda_{cmos} * \Lambda_{imspec} * G_1 * G_2}$ ayload's spectrum measurem($C = \frac{R-D}{\Lambda_{cmos} * \Lambda_{imspec} * G_1 * G_2 * \tau * g}$ er left) to corrected with dark and flat field (upper right), spectral response (lower left), and camera parameters (lower right).

4.2 Calibration Constants Calculation

In computing for the calibration constants, the resulting radiometrically corrected data in DN values is compared with the corresponding spectrum of the integrating sphere's incandescent lamp during the laboratory experiment. Since the exposure time and gain factor has already been proven to be linear against the image DN values (Lofamia, et.al., 2021), we incorporate these parameters to the final equation to correct the raw image. These values are then directly compared against the radiance values of the calibration lamp. The comparison of linearity to spectral radiance between raw DN values and the corrected DN values is seen in Figure 8.

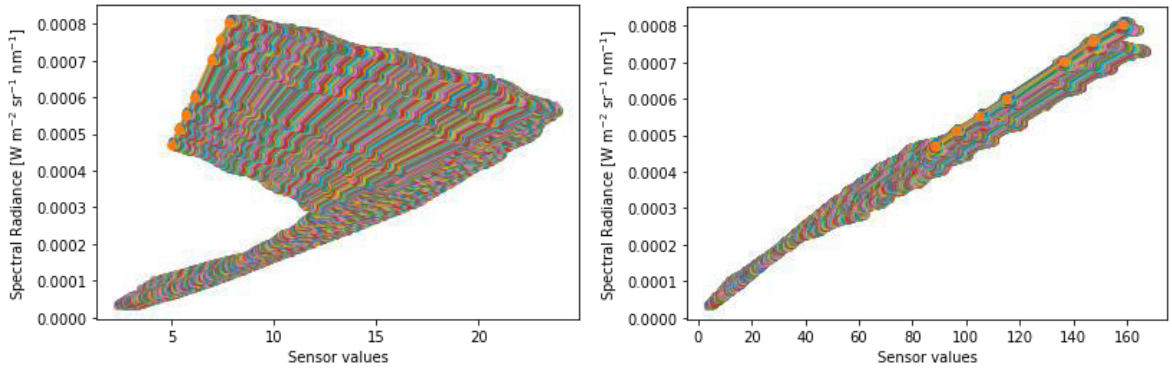

Figure 8. Raw (left) and radiometrically corrected (right) DN values vs the integrating sphere's calibration lamp's spectral radiance values.

Figure 10a shows the plotted corrected sensor values against the calibration lamp's spectral radiance. We observe a discontinuity across the line which roughly starts at 676 nm. We hypothesize that this is brought by higher order diffraction from the imaging spectrometer. Due to the mechanical modifications required, a blocking filter for the higher orders is not yet installed.

There were 3 configurations in comparing the Hypie's corrected DN and the calibration lamp's spectral radiance. Each yields a set of calibration coefficients. First, linear coefficients that are computed across all wavelengths (configuration set A). Due to the observed discontinuity, a pair of linear coefficients were each calculated for wavelengths less than 646 nm and higher than or equal to 646 nm (configuration set B). For the third configuration, a pair of coefficients were computed for each wavelength (configuration set C).

4.3 Validation

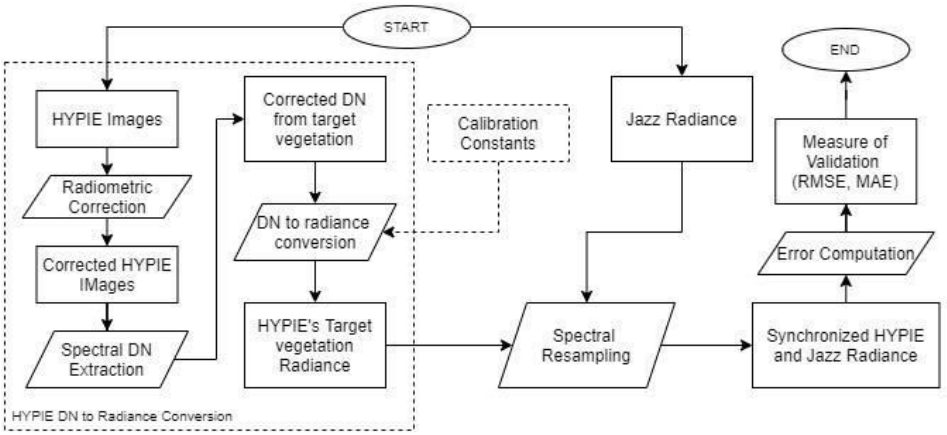

Figure 9. Workflow used to validate the calibration parameters

Due to the poor signal-to-noise ratio from the reference spectrometer for wavelengths greater than 750 nm, the validation was only done for wavelengths 450 nm to 750 nm. Calibration configuration set A, B, and C coefficients were tested against the vegetation and sun spectrum. The steps taken are summarized in Figure 9.

5. RESULTS

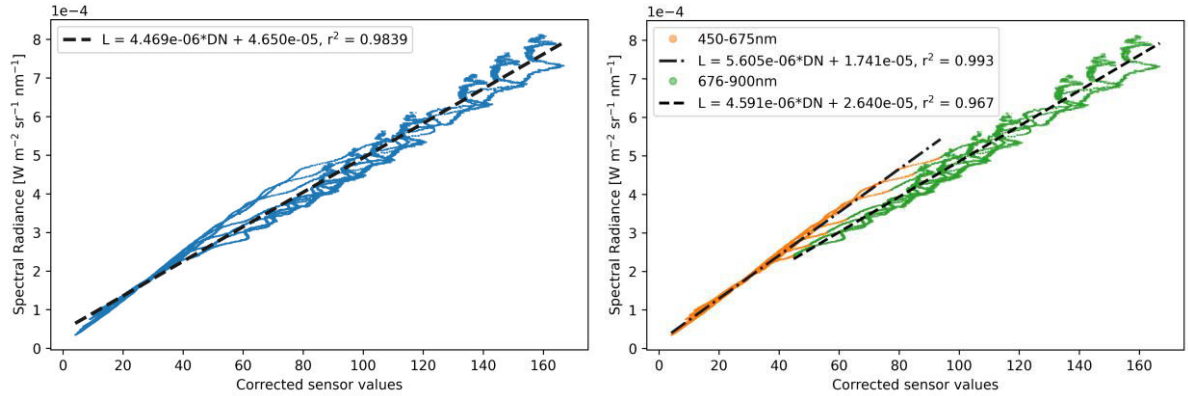

Figure 10a. Radiometric calibration for wavelength range 450-900nm, (left: calibration set A) and the observed discontinuity in spectral radiance to corrected sensor values linear relationship between shorter (450-675nm) and longer (676-900nm) wavelengths (right: calibration set B).

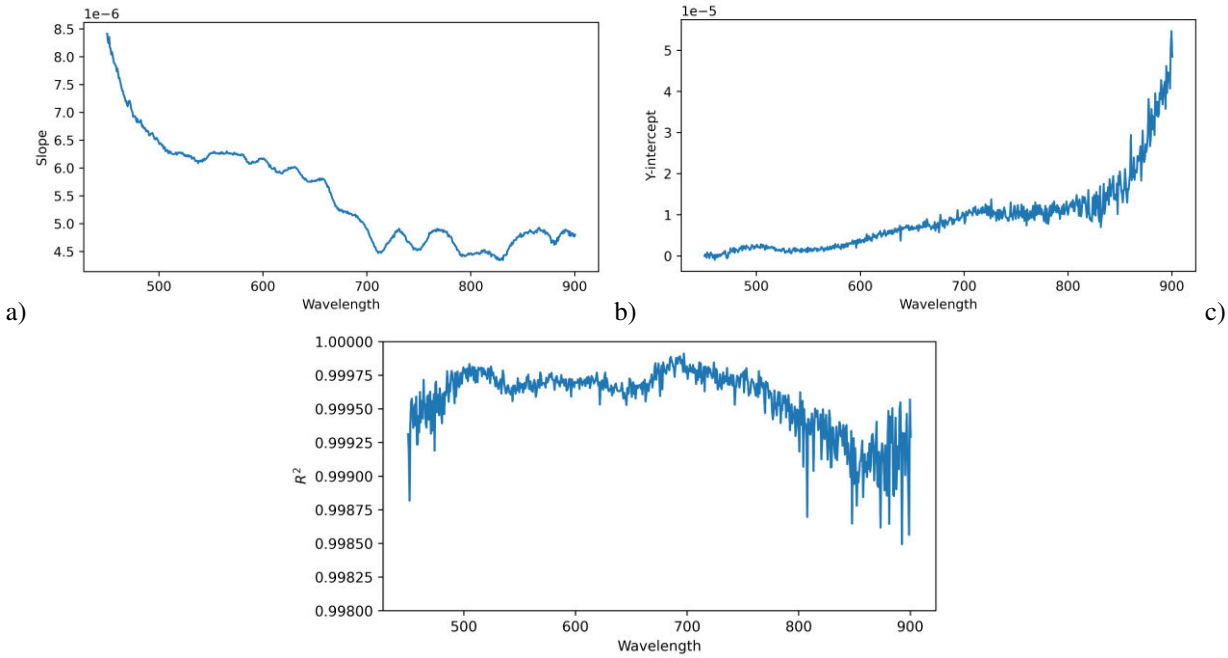

Figure 10b. Calibration coefficients for each wavelength: (a) slope and (b) y-intercept with (c) the coefficient of determination, R^2 (calibration set C).

The calibration coefficients for each configuration set, with corresponding coefficients of determination, is shown in Figure 10. The lowest coefficient of determination calculated is 0.967. These constants are applied to the Hypie's corrected DN values to convert them into radiance units.

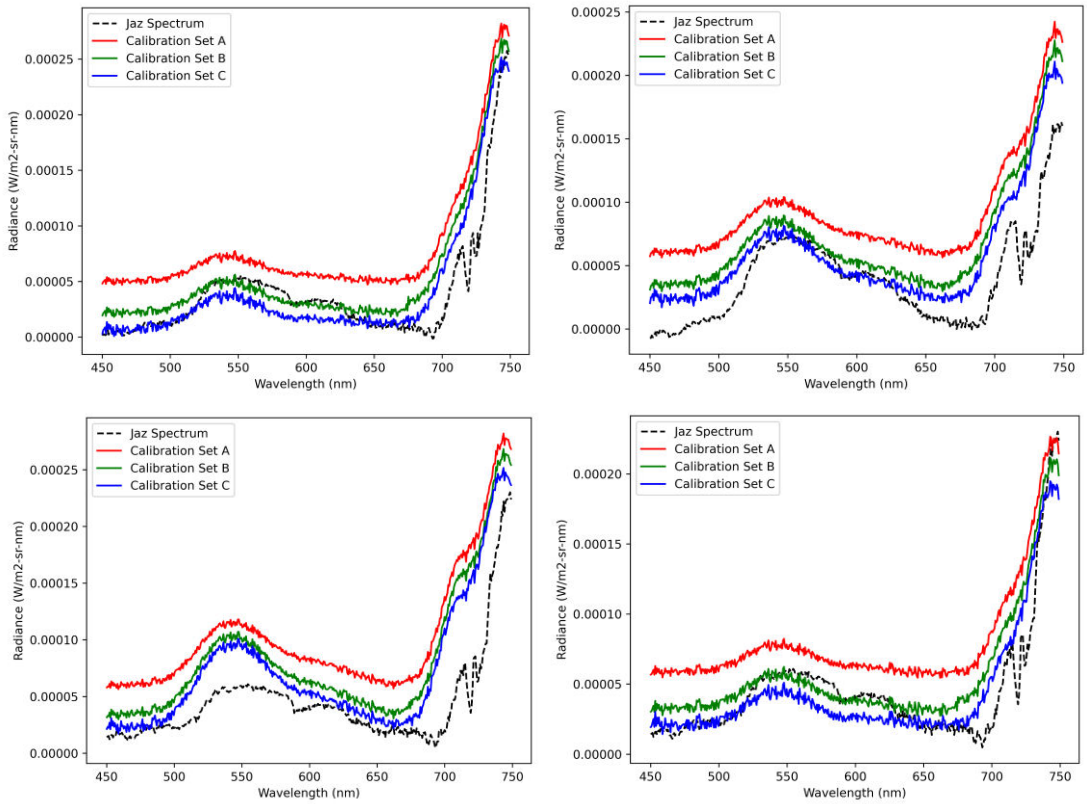

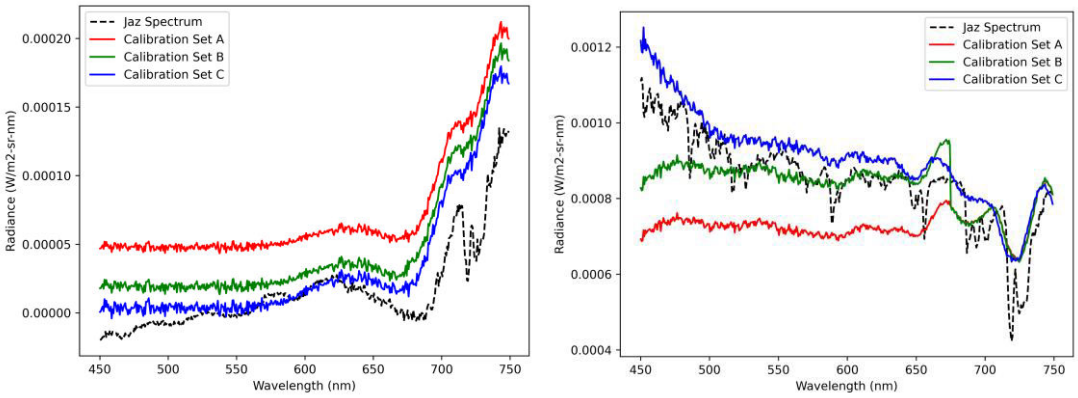

Figure 11. Jaz reference spectrometer and Hypie's spectral radiance values of the validation targets Leaf A, B, C, D, E, and sun irradiance respectively.

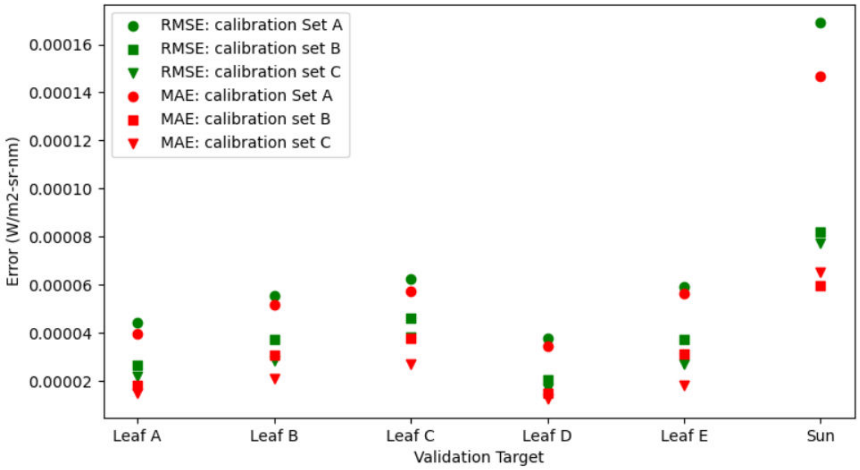

Figure 12. Error values computed for each validation target.

Figure 11 shows the resulting Hypie's spectral radiance data alongside the reference spectrometer's values. In these graphs alone, it can be observed that calibration from configurations B and C better fits the reference values. This is supported by the calculated mean absolute error and root mean square error shown in Figure 12 and Table 1.

Table 1. Summary of Errors Computed During Validation

Calibration Set	**Maximum RMSE** (x 10^{-4} W/m^2-sr-nm)	**Max Mean Abs. Error** (x 10^{-4} W/m^2-sr-nm)
A (across all wavelengths)	1.689	1.470
B (450-675 nm , 676- 900 nm)	0.821	0.599
C (per wavelength coefficients)	0.775	0.653

6. CONCLUSION

The correction done in raw Hypie images prior to the computation of calibration constants improved the data distribution between its corrected DN values and the spectral radiance of the calibration lamp. With the errors computed within acceptable values, we report to have successfully calibrated the pushbroom scanning hyperspectral sensor, Hypie. Albeit calibration set C demonstrates the lowest error values, we take into consideration that this

gives a 2-dimensional array of constants. There might be scenarios where calibration set B is more convenient to use. However, we also note that a possible spectral step at 675 nm might be a drawback in applying it.

We also recognize the limitation of working only within 450-750 nm during validation. The availability of a reference spectrometer that has reliable values within Hypie's spectral range, alongside added vegetation spectral data, will improve the reliability of the computed constants.

It is also interesting to note the discontinuity observed on Hypie's converted radiance values which we hypothesize to be caused by the imaging spectrometer's higher order diffraction beyond this region. Accounting for this discontinuity improved the recovery of spectrum as proven during validation. For future studies, we aim to eliminate the higher order diffraction during post-processing or by installing an order blocking filter, which shall enable us to improve Hypie's accuracy in acquiring absolute measurements.

ACKNOWLEDGEMENT

This study is part of the Optical Payload Technology In-depth Knowledge Acquisition and Localization (OPTIKAL) project under the Space Technology & Applications Mastery, Innovation and Advancement (STAMINA4Space) program. Project OPTIKAL is funded by the Department of Science and Technology of the Philippines - Philippine Council for Industry, Energy and Emerging Technology Research and Development (DOST - PCIEERD).

REFERENCES

Maes, W. H., & Steppe, K. (2019). Perspectives for Remote Sensing with Unmanned Aerial Vehicles in Precision Agriculture, 24(2), 152-164. https://doi.org/10.1016/j.tplants.2018.11.007

Lofamia, M. P., Maestro, M. M., Aguinaldo, R. S., Bañas, A. M., & Soriano, M. N. (2021). Payload Characterization Of An Airborne Push-broom Hyperspectral Imager [Paper presentation]. Asian Conference on Remote Sensing (also submitted), Vietnam.

Maestro, M. M., Bañas, A. M., Lofamia, M. P., Aguinaldo, R. S., Bernabe, R., Occeña, D., Toleos L., Madalipay J.T., & Soriano, M. N (2021). International Communications Satellite Systems Conference. The Institution of Engineering and Technology.